

## Seventh Workshop on the Turbulent Calculations of Sprays, TCS7

16 June, 2019 – Tenerife, Spain

### Guide for groups who intend to submit calculations for comparisons

#### A. Background

Since the inception of the TCS Workshop Series, the focus has been on dilute sprays using a number of burners which originated from Sydney, Cambridge or CORIA. While these burners are still of interest and remain on the platform of the TCS, the focus is gradually shifting to denser sprays. The Piloted Sydney Needle Burner (SYNSBURN) can provide an excellent model problem with its ability to stabilize sprays flames with liquid loadings ranging from dilute to dense. This guide provides an introduction to this burner with a description of a selected number of cases that are suggested for calculations.

#### B. THE PILOTED SYDNEY NEEDLE SPRAY BURNER:

The Sydney Piloted Needle Spray Burner (Trademark: SYNSBURN™) is designed to stabilize repeatable turbulent spray flames with a broad range of jet velocities and liquid loadings. The burner, shown schematically in Figure 1 and Figure 2, uses air-blast to atomize liquid issuing from a needle with a diameter  $D_1 = 686\mu\text{m}$ , centered in a fast co-flowing stream of air with a jet diameter,  $D = 10\text{mm}$ . The needle supplying the liquid may be recessed within the air-blast pipe so that atomization occurs upstream of the jet exit plane and hence the spray seen at the burner exit becomes less dense. The maximum recess distance is,  $L_r = 80\text{mm}$  and at this condition, the spray issuing from the jet exit plane is close to dilute. When the recess distance is zero, the dense liquid core issuing from the needle is then exposed and the spray jet is classified as dense.

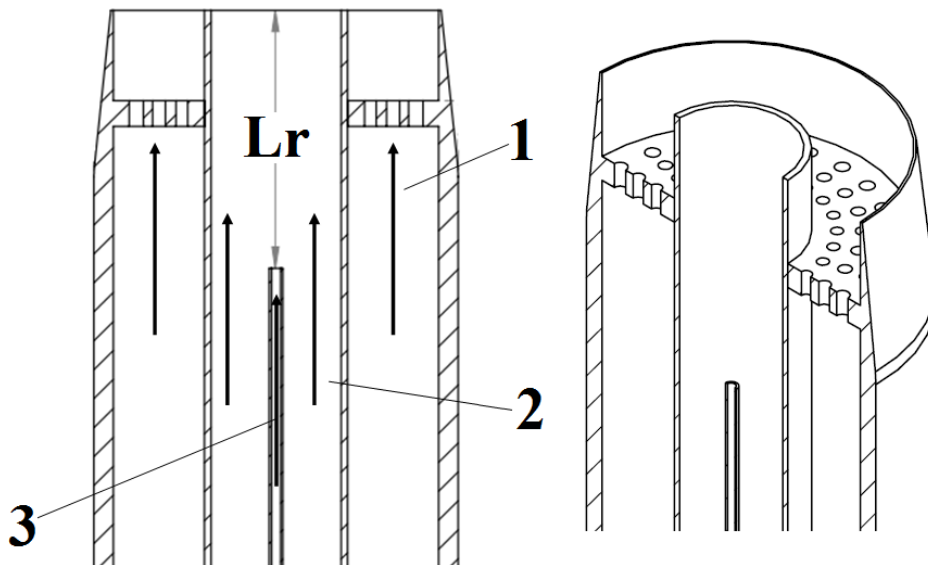
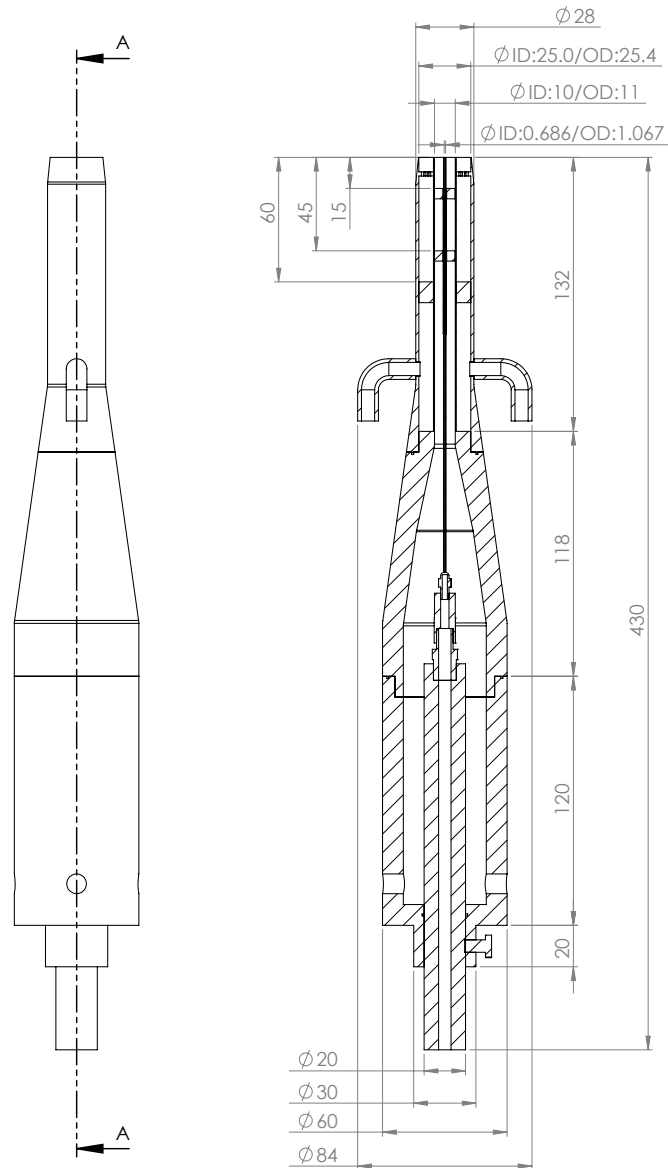


Figure 1 - Cross-section schematic of atomizer and burner tip showing the pilot stream (1), main air jet stream (2) and liquid fuel stream (3).



*Figure 2 - Full cross-section of SYNSBURN showing the dimensions of the burner for a zero recess length. The needle can be recessed a further 80-100mm, such that the burner can reach a maximum length of approximately 530mm.*

The key feature of the burner, therefore, is the ability to study a range of spray conditions from dense to dilute. This is similar, in principle, to the gaseous piloted burner which has been used earlier to investigate the effects of inlet compositional inhomogeneity on flame structure [1]–[3]. The air-blasting jet is surrounded by a pilot with an outer annulus diameter,  $D_p = 25\text{mm}$ , where premixed hydrogen  $\text{H}_2$ , acetylene  $\text{C}_2\text{H}_2$  and air issue under stoichiometric conditions with an unburnt velocity  $U_{bu}$ . The pilot composition is such that its C/H ratio is the same as that of the main fuel but with a different adiabatic flame temperature. Note that the pilot temperature could also be matched to that of the fuel with the use of diluents such as  $\text{CO}_2$  and  $\text{N}_2$  [3]. This, however, has not been done here. The pilot's main purpose is to provide a steady heat source to stabilize the main

flame to the burner surface. The entire burner assembly is mounted in a wind tunnel, providing a co-flowing air stream with a mean axial velocity of 5m/s. The tunnel exit has a cross section of 180 x 180 mm. The exit plane of the co-flow and nozzle are located 10.0 mm downstream of the exit plane of the wind tunnel. The burner has the following dimensions (Note that SYNSBURN™ can accommodate additional liquid needle diameters but only one was studied here):

- Pilot stream diameter (inner):  $D_p=25\text{mm}$  (wall thickness=0.2mm).
- Air-blast jet diameter (inner):  $D=10\text{mm}$  (wall thickness=0.5mm)
- Liquid needle diameter (inner):  $D_l=686\mu\text{m}$  (outer diameter=1067 $\mu\text{m}$ )

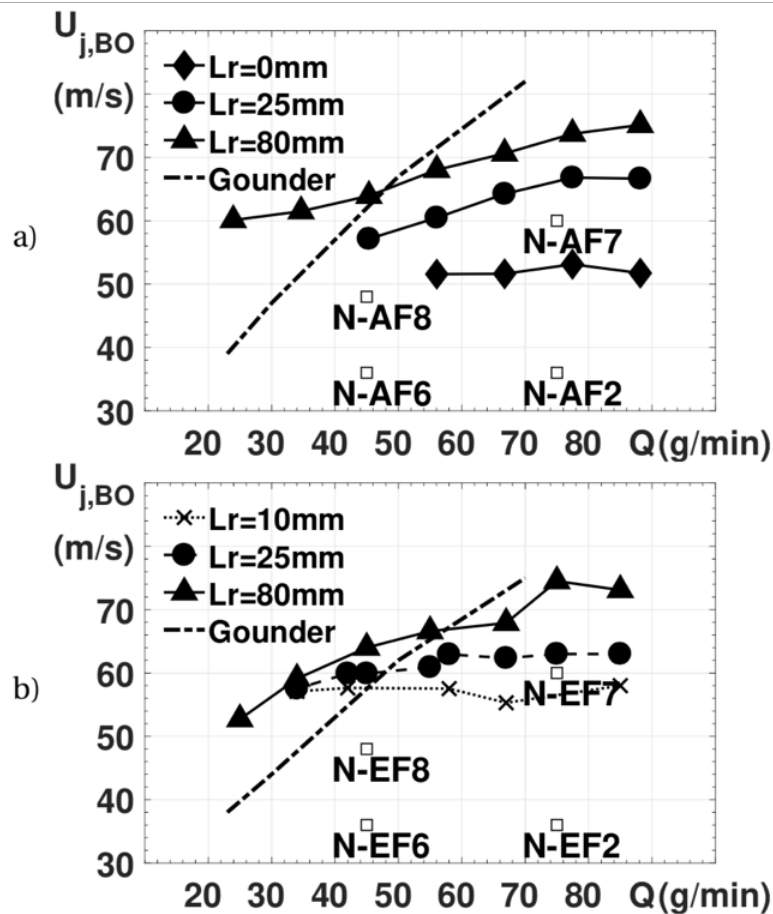


Figure 3 - Blow-off air-blast jet velocity ( $U_{BO}$ ) plotted vs. liquid a) acetone and b) ethanol mass loading ( $Q$ ) as a function of recess length ( $L_r$ ). Dashed line corresponds to equivalent dilute sprays from Gounder et al. [4]–[6] and boxes specify selected cases for further measurements

## 2. STABILITY LIMITS, MEASUREMENTS and SELECTED CASES

The parameters controlling flame stability include the recess length,  $L_r$ , the liquid mass flowrate,  $Q$  (g/min), the air-blast velocity,  $U_j$  (m/s), and the contribution of heat release from the pilot. For all the reacting cases, the pilot jet stream is maintained at stoichiometric feeding a mixture of acetylene, hydrogen and air that has the same C/H ratio as the main fuel which is 2 for acetone and 3 for ethanol. For the non-reacting cases, air is passed in the pilot stream and the bulk velocity is maintained at 1.5m/s. Flame stability limits are shown in Figure 3 for a) acetone and b) ethanol spray flames respectively, versus liquid mass loading for different recess lengths of  $L_r=0\text{mm}$ ,

25mm and 80mm. Also shown in Figure 3 are the blow-off velocities,  $U_{BO}$  reported by Gounder et al. [4]–[6] for piloted dilute spray flames of acetone and ethanol (both dashed lines). Also shown on Figure 3 are the cases selected for which data are tabulated here.

The naming methodology is explained with reference to cases N-AS2-80 and N-AF8-25: N=Needle, A=Acetone, F or S refer to flames or non-reacting sprays, respectively,  $L_r=80\text{mm}$  or  $25\text{mm}$ . The numerals in AS2 and AF8 refer to cases studied by Gounder et al. [4]–[6] and employ the same values of  $Q$  and  $U_j$ . This is intentional as it enables comparisons between established cases of dilute sprays and those studied here. Cases 2 and 6 have the same jet velocity but different liquid loading while the reverse is true for cases 6 and 8.

For comparisons of recess length for a specific case (fixed fuel loading and airblast velocity), the naming methodology is extended; for example, comparing  $LR=0, 25$  and  $80\text{mm}$  for N-AF2 will be denoted as N-AF2-0|25|80 depending on order. Likewise, comparisons of case for fixed recess length follow the same style; for example, comparing N-AF2-80, N-AF6-80 and N-AF8-80 will now be denoted as N-AF2|6|8-80. The main cases are marked by boxes in Figure 3. The exit Weber number of relevance in this burner, is defined as  $We=\rho_g U_g^2 D/\sigma$  where  $\rho_g$  is the gas density,  $U_g$  is the bulk gas velocity and  $\sigma$  is the surface tension. The fuel to air ratio is  $F/A$ ) and  $Re_g$  and  $Re_l$  refer to the Reynolds numbers of the carrier air and liquid streams, respectively.

Measurements were completed for a large matrix of cases but ONLY four are selected here for the purpose of computations at the TCS Workshop. All cases are for acetone fuel and two are reacting, namely N-AF8-80 and N-AF8-25 and two non-reacting (N-AS8-80 and N-AS8-25). Case 8 refers to an intermediate liquid loading. The recess length  $L_r=80\text{mm}$  is closer to the dilute case while  $L_r=25\text{mm}$  yields a spray case of intermediate density where filaments and liquid fragments issues from the jet exit plane. More details about the selected cases are given in Table 1:

Cases	N-AS8 N-AF8
Air jet loading (g/min)	269
Air jet velocity (m/s)	48
Air jet Reynolds number	28374
Liquid loading (g/min)	45
Liquid velocity (m/s)	2.58
Liquid Reynolds number	4180
Weber number	80
F/A ratio (by mass)	0.17
Heat release rate (kWh)	23.9
$\frac{U_j}{U_{Bo}}$ @ LR=80mm	0.75
$\frac{U_j}{U_{Bo}}$ @ LR=25mm	0.84
$\frac{U_j}{U_{Bo}}$ @ LR=0mm	N/A

Table 1 – Conditions for acetone cases N-AS8 (non-reacting) and N-AF8 (reacting) selected for the TCS7 workshop

The following measurements were performed in each dataset:

- Point measurements using Laser Doppler Velocimetry (LDV). Droplet fluxes and size distribution using Phase Doppler Anemometry (PDA). Details in [7].
- Highspeed shadowgraph imaging: classifying three types of fluid fragments used to map the evolution of sprays (droplets, ligaments and ‘irregular’ shapes). Details in [7]–[9].
- Point temperature measurements using Chirped-Probe-Pulse femtosecond Coherent anti-Stokes Raman Scattering (CPP-fs-CARS). Details in [10]–[13].

### 3. Shapes of Liquid fragments:

Backlit shadowgraph imaging of liquid fragments using microscopic lenses have results in thousands of images similar to those shown below in Fig. 4. Analysis of these complex liquid structures resulted in their classification in the following three broad categories which are shown in Fig. 5: spherical (and slightly non-spherical) droplets, ‘ligaments’ estimated to be elongated ellipsoids, and ‘large objects’ that are generally irregular.

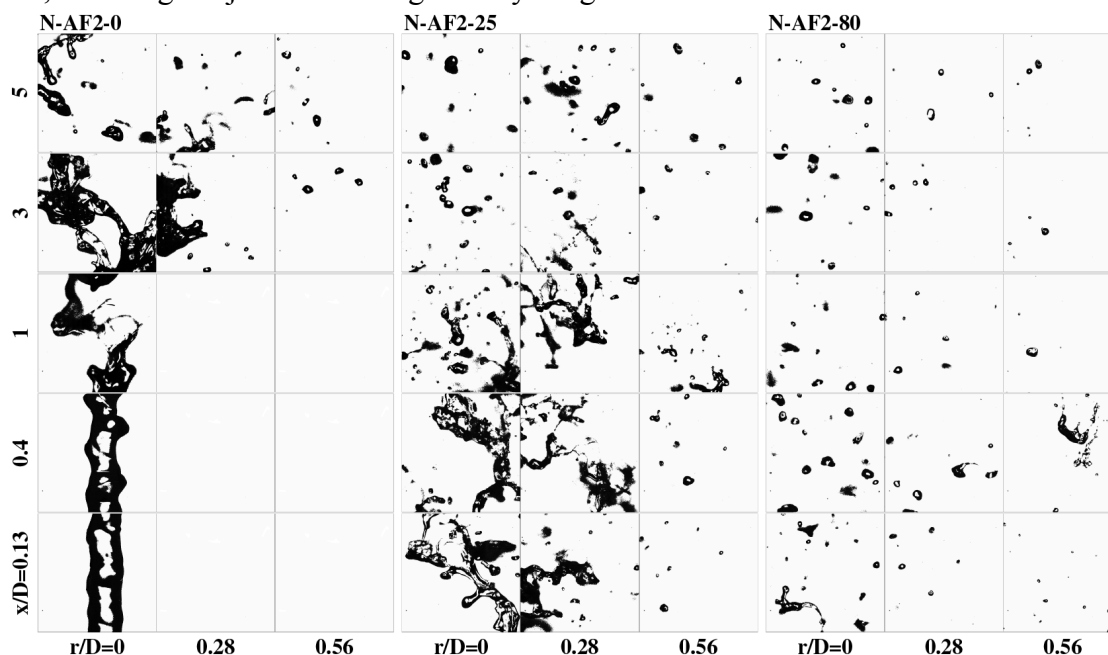


Fig. 4 - Representative snapshots of acetone spray fragments for reacting N-AF2 from  $x/D=0.13-5$  across the spray cross section comparing recess lengths 0, 25 and 80mm; a superficial threshold was applied for clarity (note:  $x/D$  locations align with bottom of each measurement window,  $r/D$  locations align with centerline of each measurement window)

These structural categories (see Fig. 5) are nominally (and somewhat pragmatically) defined in terms of their aspect ratio,  $AR$ , characteristic major axis length,  $d_{max}$  and the initial liquid jet diameter,  $D_l=686\mu\text{m}$ , as follows:

- Droplets ( $d_{max} < D_l$  and  $AR < 3$ )
- Ligaments ( $AR > 3$ )
- ‘Irregular’ objects ( $d_{max} > D_l$  and  $AR > 3$ )

The identification of these structures is automated by developing advanced image processing routines which are validated using data collected in simpler, well-known flows. The choice of a threshold of  $AR=3$  is purely arbitrary but useful limit do delineate between distorted sphere and elongated ligaments. The developed routines are then applied to the thousands of images collected here to obtain statistics on the relative abundance of each category of fragments. Only population

distributions and surface areas are obtained and reported since full volume information requires three dimensional data which is not yet available. A sample of the fragment statistics that may be derived from the reported measurements and the classification described here is shown in Fig. 6.

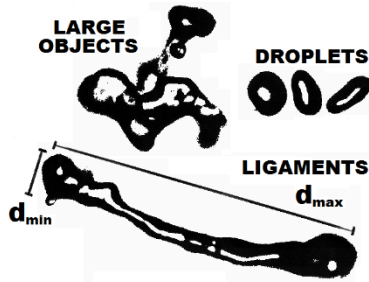


Fig. 5 - Illustrations of droplets, ligaments and unbroken 'irregular' objects.

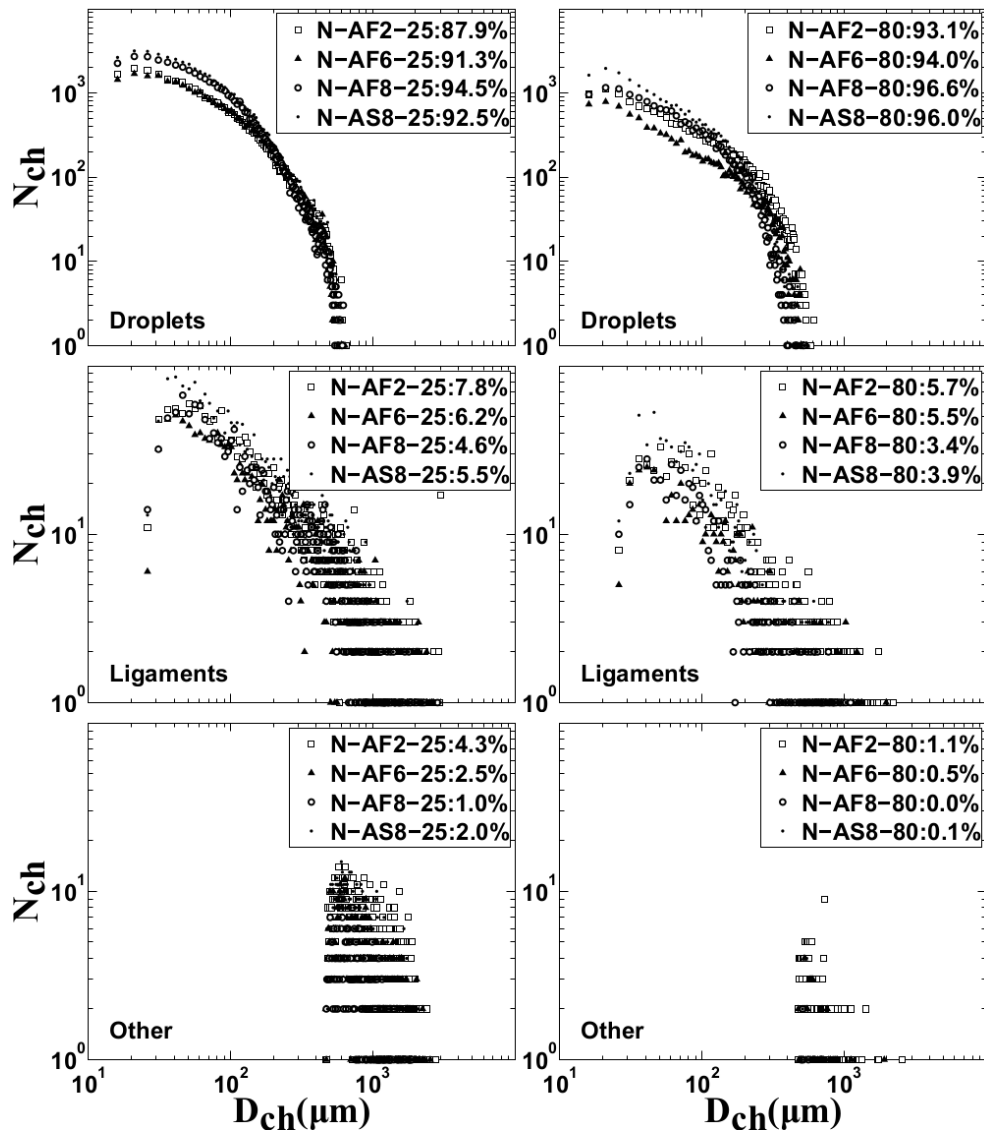


Fig. 6 - Population distributions  $N_{ch}$  of characteristic size  $D_{ch}$  for all liquid shape classifications with a recess length 25mm (left) and 80mm (right) at the centreline of the exit plane ( $x/D=0.13$ ) for various cases. Each inset provides the percentage of each shape category against total detected objects ( $N_{ch}/N_{tot}$ )

#### **4. Boundary Conditions**

Detailed boundary conditions are provided for the turbulent spray jets and flames including velocity and droplets fields at the jet exit plane, fragment statistics, and temperature profiles (for the reacting cases). The boundary conditions for the selected cases are listed below:

##### 4.1 Velocity of gas and droplets fluxes in the jet:

These are obtained using the LDV/PDA technique as close to the burner surface ( $x/D=0$ ) as possible, in this case the measurements are taken at  $x/D=0.3$ . These are then conditioned with respect to the droplet size so that gas field velocities refer to measurement of droplet with diameters  $<10\mu\text{m}$ .

*SYNSBURN Boundary Conditions (BC) => "LDV/PDA BC"*

##### 4.2 Temperature:

These are obtained using the CPP-fs-CARS technique as close to the burner surface ( $x/D=0$ ) as possible, in this case the measurements are taken at  $x/D=0.4$  as follows:

*SYNSBURN Boundary Conditions (BC) => "CPP-fs-CARS BC"*

##### 4.3 Fragment Statistics:

These are obtained from the high-speed shadowgraph images as close to the burner surface ( $x/D=0$ ) as possible, in this case the measurements are taken at  $x/D=0.13$  as follows:

*SYNSBURN Boundary Conditions (BC) => "Shadowgraph BC"*

Now for the pilot stream, velocities are estimated from the bulk flow and the equilibrium temperature in the pilot. For the co-flow wind tunnel, LDV measurements of velocity profiles made when the tunnel was seeded with droplets issued from a smoke machine using mono-propylene/triethylene glycol mixture as working fluid. The measurements in the co-flowing stream were made using the following conditions:

Wind Tunnel Air Velocity = 5m/s

Bulk Velocity in pilot stream (air only) = 4.5m/s

The central jet had air flowing at velocities similar to those in cases similar to flow in cases 2, 6, 7 and 8.

Radial profiles of mean velocity and turbulence in the co-flow are given in:

*SYNSBURN: Boundary Conditions (BC) => "SYNSBURN Windtunnel Velocity BC.xlsx"*

Note: in the tabulated velocity data, channel 1 refers to the axial velocity component and channel 2 refer to radial velocity.

#### **5. SPRAY FLAMES OF ACETONE**

Here is a list of the tabulated data set that is made available for the TCS. The more complete data is available on the web and may be available with pass word access (please contact Assaad Masri if you

need access to the full data set. It is recommended to study the README files to better understand the format of the data before going further.

- **LDV/PDA**

SYNSBURN LDV/PDA => "SYNSBURN: LDV/PDA Dataset"

- **Highspeed Shadowgraph Imaging**

SYNSBURN Shadowgraph => "SYNSBURN: Shadowgraph Dataset"

- **CPP-fs-CARS**

SYNSBURN CPP-fs-CARS => "SYNSBURN: CPP-fs-CARS Dataset"

## **REFERENCES:**

- [1] R. S. Barlow, S. Meares, G. Magnotti, H. Cutcher, and A. R. Masri, "Local extinction and near-field structure in piloted turbulent CH<sub>4</sub>/air jet flames with inhomogeneous inlets," *Combust. Flame*, vol. 162, no. 10, pp. 3516–3540, Oct. 2015.
- [2] S. Meares, V. N. Prasad, G. Magnotti, R. S. Barlow, and A. R. Masri, "Stabilization of piloted turbulent flames with inhomogeneous inlets," *Proc. Combust. Inst.*, vol. 35, no. 2, pp. 1477–1484, 2015.
- [3] H. C. Cutcher, R. S. Barlow, G. Magnotti, and A. R. Masri, "Turbulent flames with compositionally inhomogeneous inlets: Resolved measurements of scalar dissipation rates," *Proc. Combust. Inst.*, vol. 36, no. 2, pp. 1737–1745, 2017.
- [4] J. D. Gounder, A. Kourmatzis, and A. R. Masri, "Turbulent piloted dilute spray flames: Flow fields and droplet dynamics," *Combust. Flame*, vol. 159, no. 11, pp. 3372–3397, 2012.
- [5] A. R. Masri and J. D. Gounder, "Turbulent spray flames of acetone and ethanol approaching extinction," *Combust. Sci. Technol.*, vol. 182, no. 4, pp. 702–715, 2010.
- [6] S. H. Stårner, J. Gounder, and A. R. Masri, "Effects of turbulence and carrier fluid on simple, turbulent spray jet flames," *Combust. Flame*, vol. 143, no. 4, pp. 420–432, Dec. 2005.
- [7] A. Lowe, A. Kourmatzis, and A. R. Masri, "Turbulent spray flames of intermediate density: Stability and near-field structure," *Combust. Flame*, vol. 176, pp. 511–520, 2017.
- [8] A. Kourmatzis, P. X. Pham, and A. R. Masri, "Air assisted atomization and spray density characterization of ethanol and a range of biodiesels," *Fuel*, vol. 108, no. 0, pp. 758–770, 2013.
- [9] A. Kourmatzis, P. X. Pham, and A. R. Masri, "Characterization of atomization and combustion in moderately dense turbulent spray flames," *Combust. Flame*, vol. 162, no. 4, pp. 978–996, 2015.
- [10] A. Lowe, L. M. Thomas, A. Satija, R. P. Lucht, and A. R. Masri, "Chirped-probe-pulse femtosecond CARS thermometry in turbulent spray flames," *Proc. Combust. Inst.*, vol. 37, no. 2, pp. 1383–1391, Jan. 2019.
- [11] L. M. Thomas, A. Lowe, A. Satija, A. R. Masri, and R. P. Lucht, "Five kHz thermometry in turbulent spray flames using chirped-probe pulse femtosecond CARS, part I: Processing and interference analysis," *Combust. Flame*, vol. 200, pp. 405–416, Feb. 2019.
- [12] A. Lowe, L. M. Thomas, A. Satija, R. P. Lucht, and A. R. Masri, "Five kHz thermometry in turbulent spray flames using chirped-probe-pulse femtosecond CARS, part II: Structure of reaction zones," *Combust. Flame*, vol. 200, pp. 417–432, Feb. 2019.
- [13] L. M. Thomas, A. Satija, and R. P. Lucht, "Technique developments and performance analysis of chirped-probe-pulse femtosecond coherent anti-Stokes Raman scattering combustion thermometry," *Appl. Opt.*, vol. 56, no. 31, pp. 8797–8810, Nov. 2017.